Nuclear Engineering and Technology 55 (2023) 4238–4245

Contents lists available at ScienceDirect

Nuclear Engineering and Technology

journal homepage: www.elsevier.com/locate/net

Original Article

A novel radiation-dependence model of InP HBTs including gamma radiation effects☆

Jincan Zhang [a,*], Haiyi Cai [a], Na Li [a], Liwen Zhang [a], Min Liu [a], Shi Yang [b]

[a] Electrical Engineering College, Henan University of Science and Technology, Luoyang, 471023, China
[b] Novaco Microelectronics Technologies Ltd., Nantong, 226000, PR China

ARTICLE INFO

Keywords:
Compact model
Gamma radiation effects
InP heterojunction bipolar transistors
Advanced design system software

ABSTRACT

In order to predict the lifetime of InP Heterojunction Bipolar Transistor (HBT) devices and related circuits in the space radiation environment, a novel model including gamma radiation effects is proposed in this paper. Based on the analysis of radiation-induced device degradation effects including both DC and AC characteristics, a set of empirical expressions describing the device degradation trend are presented and incorporated into the Keysight model. To validate the effective of the proposed model, a series of radiation experiments are performed. The correctness of the novel model is validated by comparing experimental and simulated results before and after radiation.

1. Introduction

Even though III-V compound semiconductors are versatile and have been applied to various kinds of electronics devices drawing nearly equivalent attention as Si-based technology and devices, major technical difficulties in the fabrication and engineering of III-V heterostructure devices were not solved until molecular beam epitaxy (MBE) and metal organic chemical vapor deposition (MOCVD) growth techniques were developed. Owing to the possibility of controlling the bandgap of material during the material grown and with the excellent electron transport properties, a large number of InP-based devices have been studied in various fields exhibiting superior properties for high-speed circuits/ devices applications [1–4].

InP heterojunction bipolar transistors (HBTs) technology has generated considerable interest in the space community because of its robustness to radiation without any additional hardening [5,6]. Consisting of highly sophisticated electronic systems requiring expensive preparing, launching, and maintaining the satellite-based resource, the issues related to the reliability and lifetime of the electronics systems on board the satellite deserve careful consideration, so it is important to investigate radiation effects on electronics systems in terms of degradation mechanisms as well as radiation model being used to predict the lifetime of InP HBTs.

Main applications of HBTs are in high performance lightweight electronics communication systems used in military and space satellites. The recent boost of wireless and other high-end communications continues to draw more and more attention to reliable long-term performance of HBTs devices under radiation. Previous experimental studies showed that HBTs show superior resistivity to electron [7], gamma [8–11] and neutron [12,13] radiations comparing to that of high-performance Si BJTs. Radiation effects on HBTs devices induced by ion [14–17] and proton [18–22] irradiation have also been reported by several groups. Theoretical work so far has been mostly focus on the radiation-induced degradation results and degradation mechanisms studied used the physical Technology Computer Aided Design (TCAD) [23–27], very few touching establishment of compact models including radiation effect [28,29]. Establishing the model-accurately radiation models responsible for the radiation-induced degradation is important for the development of improved radiation-hard devices/circuits designs. There are some works for studying radiation-induced degradation effect by compact models [8,30]. However, there is very little report for modeling the degradation characteristics as a function of radiation dose based on compact models. Although the Vertical Bipolar Inter-Company (VBIC) model considering the radiation effects of gallium arsenide (GaAs) HBTs was studied in our previous published work [31], no study has been made to establish compact models including radiation effects

☆ This work was supported by the National Natural Science Foundation of China (Grant No: 61804046), the Foundation of Department of Science and Technology of Henan Province (Grant No. 222102210172, 222102210207, 212102210286), and the Foundation of He'nan Educational Committee (Grant No. 20B510006).

* Corresponding author.
E-mail address: zjc850126@163.com (J. Zhang).

https://doi.org/10.1016/j.net.2023.07.045
Received 30 August 2021; Received in revised form 29 May 2023; Accepted 31 July 2023
Available online 25 August 2023
1738-5733/© 2023 Korean Nuclear Society. Published by Elsevier B.V. This is an open access article under the CC BY-NC-ND license (http://creativecommons.org/licenses/by-nc-nd/4.0/).

of InP HBTs based on the Keysight model, which is studied in this work. The Keysight model was developed specifically for GaAs and InP HBTs, describing the electrical behaviors of III-V HBTs more precisely than the VBIC model. Additionally, the model in Ref. [31] only considers the degradations in forward base current and cutoff frequency, not the degradations of forward collector current, inverse Gummel currents and junction capacitances. However, these degradations appeared after radiation in InP HBTs, which are also considered in the proposed model.

In this paper, a novel model including radiation effects for InP HBTs on the basic of the Keysight model is proposed. This paper is organized as follows. The radiation model for implementation of radiation effects of InP HBTs is developed in Section II. In order to verify the rationality of the model, the modeled results are given and analyzed in Section III, and the conclusions are summarized in Section IV.

2. Model

Several models that are specifically based on modern HBT devices (VBIC model, Keysight model, and HiCUM model) have been developed in an attempt to give more accurate large-signal modeling and more reliable circuit designs. The Keysight model has been shown to be especially good at modeling HBTs characteristics [32]. The detailed description for the Keysight model can be found in Ref. [33]. The model however lacks radiation dependence, limiting circuit designs to the use of device at non-radiation environment. Unfortunately, HBTs have been widely used in the space radiation environment. Forward Gummel characteristics and cutoff frequency are significantly degraded when exposed to radiation, additionally, inverse Gummel characteristics and junction capacitances also show slight degradation after radiation in our previous study [33].

2.1. Forward Gummel

After radiation, prominent degradation of forward base current I_{BE} occurs, and there is slight increase for forward collector current I_{CC}. To accurately reflect these degradations, the variations of saturation currents and ideal factors versus radiation total dose could be included. Therefore, I_{BE} and I_{CC} after radiation can be induced as equations (1) and (2), respectively.

$$I_{BE_rad} = (q_{3\ mod})^{G_{KDC}} \times (I_{SH} + \Delta I_{SH})\left(\exp\left(\frac{V_{BE}}{(N_H + \Delta N_H) \times V_{TV}}\right) - 1\right) + (I_{SE} + \Delta I_{SE})\left(\exp\left(\frac{V_{BE}}{(N_E + \Delta N_E) \times V_{TV}}\right) - 1\right) \tag{1}$$

$$I_{CC_rad} = \frac{(I_S + \Delta I_S)\left(\exp\left(\frac{V_{BE}}{(N_F + \Delta N_F) \times V_{TV}}\right) - 1\right)}{D_D \times q_{3\ mod}} \tag{2}$$

where ΔI_{SH} and ΔN_H are excess forward ideal base saturation current and ideal factor, respectively. ΔI_{SE} and ΔN_E are excess forward non-ideal base saturation current and ideal factor, respectively. ΔI_S and ΔN_F are excess forward collector saturation current and ideal factor, respectively. And other parameters descriptions can be found in Ref. [33].

2.2. Inverse Gummel

Inverse base current I_{BC} in low voltage-bias regime are slight degraded, while inverse emitter current appears to be no change when HBT is exposed to radiation. In addition, the slope of I_{BC} in low voltage-bias regime stays constant before and after radiation [33]. Therefore, we could only insert a parameter ΔI_{SC} reflecting the degradation of inverse non-ideal base saturation current I_{SC}. The expression of I_{BC} can be improved as equation (3).

$$I_{BC_rad} = I_{SRH}\left(\exp\left(\frac{V_{BC}}{N_{RH} \times V_{TV}}\right) - 1\right) + (I_{SC} + \Delta I_{SC})\left(\exp\left(\frac{V_{BC}}{N_C \times V_{TV}}\right) - 1\right) \tag{3}$$

where the descriptions of parameters in equation (3) can be found in Ref. [33].

2.3. Junction capacitances

Junction capacitances of InP HBTs appear to slight degrade after radiation in our previous study, which is different from non-change of junction capacitances for GaAs HBTs in Ref. [31]. Because these degradations of junction capacitances for InP HBTs are very slight, we could only change base-emitter zero-bias capacitance C_{JE} and base-collector zero-bias capacitance C_{JC} to reflect the degradation of base-emitter capacitance C_{BE} and the degradation of base-collector capacitance C_{BC}, respectively. Therefore, the expressions of C_{JE} and C_{JC} after radiation can be improved as equations (4) and (5), respectively.

$$C_{JE_rad} = C_{JE} + \Delta C_{JE} \tag{4}$$

$$C_{JC_rad} = C_{JC} + \Delta C_{JC} \tag{5}$$

where ΔC_{JE} and ΔC_{JC} are radiation-induced excess base-emitter zero-bias capacitance and excess base-collector zero-bias capacitance, respectively.

2.4. Cutoff frequency

Physically, the expression of cutoff frequency F_T can be shown as:

$$F_T = \frac{1}{2\pi(\tau_e + \tau_b + \tau_{sc} + \tau_c)} \tag{6}$$

$$\tau_e = \frac{V_{TV}}{I_C} \cdot (C_{BE} + C_{BC}) \tag{7}$$

$$\tau_c = (R_E + R_C) \cdot C_{BC} \tag{8}$$

where the description of parameters in equation (6) can be obtained in Ref. [33]. In Eq. (7), I_C is collector current of HBTs. In Eq. (8), R_E and R_C are emitter resistance and collector resistance, respectively. In the Keysight model, the transit time is just the sum of τ_b and τ_{sc}.

In our previous study [33], it can be seen that resistances are not degraded, meanwhile junction capacitances appear to very slight increase after radiation. Therefore, we have enough reasons to believe that the degradation of F_T is caused by the increase of junction capacitances together with the increase of transit time. The degradation of the transit time is mainly caused by displacement-induced acceptor deactivation in the base region of the devices, so we can insert a parameter ΔT_{fb} related to the variation of the intrinsic base transit-delay time T_{fb}, to reflect the degradation the transit time, in turn to describe the change of F_T. In this case, T_{fb} can be improved as equation (9).

$$T_{fb_rad} = T_{fb} + \Delta T_{fb} \tag{9}$$

3. Experiment and analysis

In order to evaluate the electrical characteristics of integrated circuits for an established radiation dose, comprehensive models for both radiation effects and device operation are needed. The improved Keysight model including radiation effects were implemented by use of symbolically defined device (SDD) in Advanced Design System (ADS) software.

The InP HBTs used in this study were grown by the Institute of Microelectronics in the Chinese Academy of Sciences. The schematic

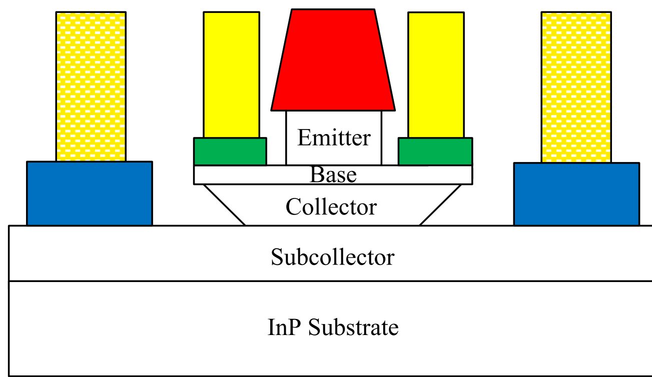

Fig. 1. Schematic diagram of the investigated InP HBT.

diagram of the HBTs can be found in Fig. 1. The structure consists of a 300-nm InP (Si: 3×10^{19}cm^{-3}) and a 25-nm $In_{0.53}Ga_{0.67}As$ (Si: 3×10^{19}cm^{-3}) and a 50-nm InP (Si: 1.2×10^{19}cm^{-3}) as subcollector, a 160-nm InP (Si: 2×10^{16}cm^{-3}) as the collector, a 10-nm $In_{0.88}Ga_{0.12}As_{0.27}P_{0.73}$ (Eg = 1.15 eV), a 10-nm $In_{0.73}Ga_{0.27}As_{0.58}P_{0.42}$ (Eg = 0.95 eV) and a 20-nm $In_{0.53}Ga_{0.47}As$ (Si: 2×10^{16}cm^{-3}) as the grade layer, a 40-nm InGaAs base layer (C: 4×10^{19}cm^{-3}), a 60-nm InP emitter (Si: 3×10^{17}cm^{-3}), and a 100-nm InP (Si: 3×10^{19}cm^{-3}) and 200-nm $In_{0.53}Ga_{0.67}As$ cap layer (Si: 3×10^{19}cm^{-3}). Gamma irradiation experiment was performed by using 60Co gamma source at the rate of about 0.182 Mrad(Si) per hour, and continuous irradiation time 5.5 h, 16.5 h, 38.5 h, and 55 h, corresponding to 1 Mrad(Si), 3 Mrad(Si), 7 Mrad(Si), and 10 Mrad(Si) gamma irradiation total dose. In the process of irradiation experiment, these HBT devices were unbiased and left floating at the ambient temperature.

Measured DC data are acquired using an HP4142B modular DC source, and S-parameters data are characterized with an HP8510C network analyzer from 0.1 to 40 GHz. The devices were measured using Ground-Signal-Ground (GSG) microwave probes with 150 μm pitch between the ground and signal probe tips. To confirm measurement accuracy of the devices reported in this work, there are 6 devices under each irradiation dose point and the differences of features among all of the 24 devices are within 0.2%.

The extraction and verification of the proposed model are performed on a 1×15 μm^2 emitter area InP HBT device. The model parameters extraction procedure begins with the extraction of the pad parasitic elements: the parasitic capacitances and inductances. This can be done from the measured *S*-parameters of de-embedding open and short test structures, and then the extracted pad parasitic parameters are de-embedded from the measured S-parameters to yield the intrinsic *S*-parameters. After de-embedding, the series resistances (R_B, R_C, R_E) can be extracted using the open-collector method [34], and the extracted values of resistances are shown in Table 1.

3.1. Forward Gummel

The values of I_{SE} and N_E parameters can be extracted by fitting the y-axis intercept and slope of the log(I_{BE}) versus V_{BE} curve in the low V_{BE} regime. In the high V_{BE} bias range, I_{SH} and N_H are then determined from the y-axis intercept and slope in forward Gummel base current I_{BE} plot. Similarly, the I_S and N_F parameters can also be easily determined using a linear regression in forward Gummel collector current I_{CC} curve. The extracted values of I_{SE}, N_E, I_{SH}, N_H, I_S, and N_F parameters are given in Table 1 before radiation and after radiation.

The calculated curves of ΔI_{SE}, ΔN_E, ΔI_{SH}, and ΔN_H varying with radiation dose levels are shown in Fig. 2. Since the curves start to saturate with the increase of radiation dose level, to predict the degradation of I_{BE} after radiation, the exponential function expressions are adopted to describe ΔI_{SE}, ΔN_E, ΔI_{SH}, and ΔN_H:

$$\Delta I_{SE} = a_{SE} + b_{SE} \cdot \exp(c_{SE} \cdot D) \tag{10}$$

$$\Delta N_E = a_E + b_E \cdot \exp(c_E \cdot D) \tag{11}$$

$$\Delta I_{SH} = a_{SH} + b_{SH} \cdot \exp(c_{SH} \cdot D) \tag{12}$$

$$\Delta N_H = a_H + b_H \cdot \exp(c_H \cdot D) \tag{13}$$

where a_{SE}, b_{SE}, c_{SE}, a_E, b_E, c_E, a_{SH}, b_{SH}, c_{SH}, a_H, b_H, c_H are fitting parameters, and D is radiation dose level.

The modeled forward base current I_{BE} agrees well with the measured results under all radiation doses, and the error between the modeled and measured results is less than 1.5%, as drawn in Fig. 2. From Fig. 3, it is evident that the forward Gummel base current I_{BE} shows significant increase in the low bias range, and at the high current levels I_{BE} also appear to slight degradation. The accuracy of the proposed model is higher than the model presented in Ref. [31], for which, there are two established reasons. On one hand, the Keysight model describes device characteristics more accurately than the VBIC model. On the other hand, the proposed model takes account of the degradations of I_{SH} and N_H associating with the neutral base region.

The objective functions for modeling ΔI_S and ΔN_F parameters are

Table 1
Extracted values of Keysight model critical DC parameters before and after irradiation.

	Parameters	Pre-radiation	Post-radiation of 1 Mrad(Si)	Post-radiation of 3 Mrad(Si)	Post-radiation of 7 Mrad(Si)	Post-radiation of 10 Mrad(Si)
forward Gummel	I_S (A)	1.015×10^{-14}	1.11×10^{-14}	1.251×10^{-14}	1.368×10^{-14}	1.390×10^{-14}
	N_F	1.167	1.1679	1.1692	1.1712	1.172
	I_{SH} (A)	6.018×10^{-17}	7.3946×10^{-17}	9.702×10^{-17}	1.1247×10^{-16}	1.151×10^{-16}
	N_H	1.134	1.138	1.1455	1.15	1.151
	I_{SE} (A)	5.598×10^{-14}	1.06047×10^{-12}	3.046×10^{-12}	5.605×10^{-12}	7.478×10^{-12}
	N_E	1.665	1.972	2.0708	2.129	2.166
inverse Gummel	I_{SR}(A)	5.7×10^{-16}	5.7×10^{-16}	5.7×10^{-16}	5.7×10^{-16}	5.7×10^{-16}
	N_R	0.918	0.918	0.918	0.918	0.918
	I_{SRH} (A)	7.757×10^{-12}	7.757×10^{-12}	7.757×10^{-12}	7.757×10^{-12}	7.757×10^{-12}
	N_{RH}	1.287	1.287	1.287	1.287	1.287
	I_{SC} (A)	1.696×10^{-9}	1.958×10^{-9}	2.491×10^{-9}	2.919×10^{-9}	3.084×10^{-9}
	N_C	2.186	2.186	2.186	2.186	2.186
series resistances	R_E (Ω)	1.64	1.64	1.64	1.64	1.64
	R_{CI} (Ω)	6.545	6.545	6.545	6.545	6.545
	R_{CX} (Ω)	3.7	3.7	3.7	3.7	3.7
	R_{BI} (Ω)	1.1	1.1	1.1	1.1	1.1
	R_{BX} (Ω)	5.97	5.97	5.97	5.97	5.97
	R_{TH1} (Ω)	240	240	240	240	240
	R_{TH2} (Ω)	0	0	0	0	0

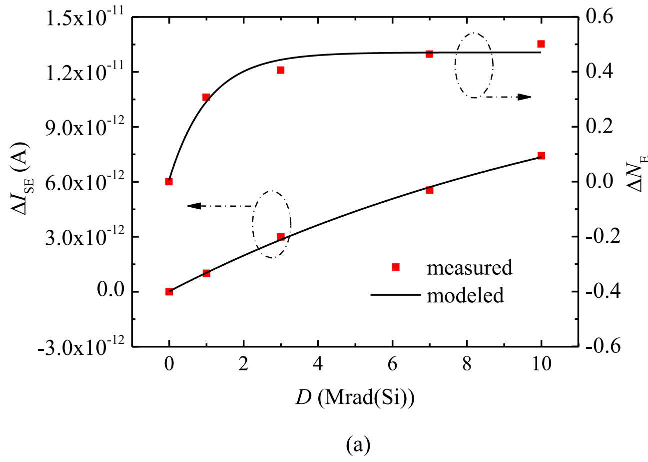

(a)

(b)

Fig. 2. Measured and modeled results for (a) ΔI_{SE} and ΔN_E, (b) ΔI_{SH} and ΔN_{SH}.

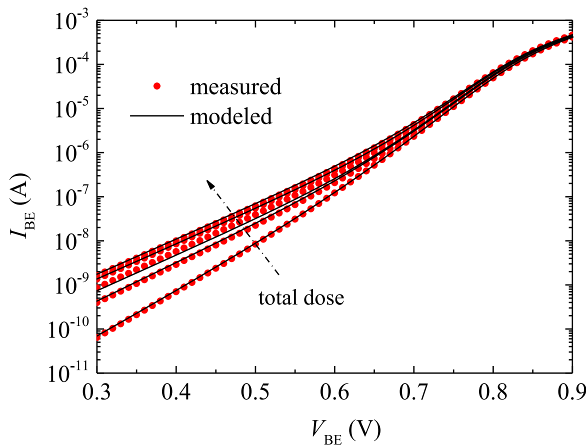

Fig. 3. Measured and modeled results of I_{BE} under different total dose levels.

expressed as equations (14) and (15), respectively, where a_S, b_S, c_S, a_F, b_F, and c_F are fitting parameters. The measured and modeled curves of ΔI_S and ΔN_F versus radiation dose level are shown in Fig. 4. The error between the measured forward Gummel collector I_{CC} and modeled result is less than 1% for all radiation doses, as shown in Fig. 5. Thus, it can be concluded that the proposed model can precisely predict the degradations of the forward Gummel current.

$$\Delta I_S = a_S + b_S \cdot \exp(c_S \cdot D) \tag{14}$$

$$\Delta N_F = a_F + b_F \cdot \exp(c_F \cdot D) \tag{15}$$

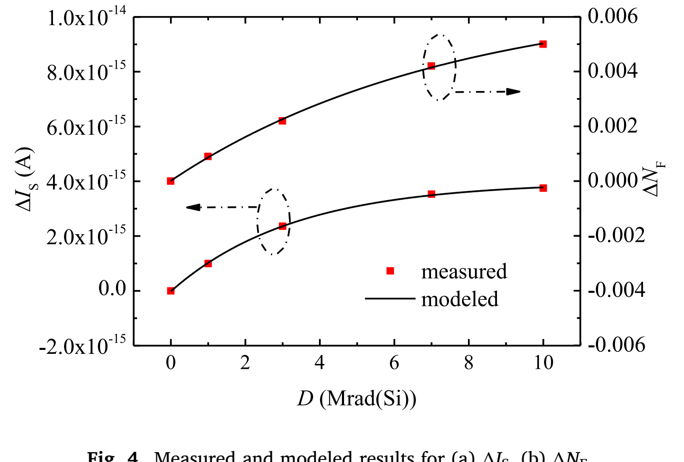
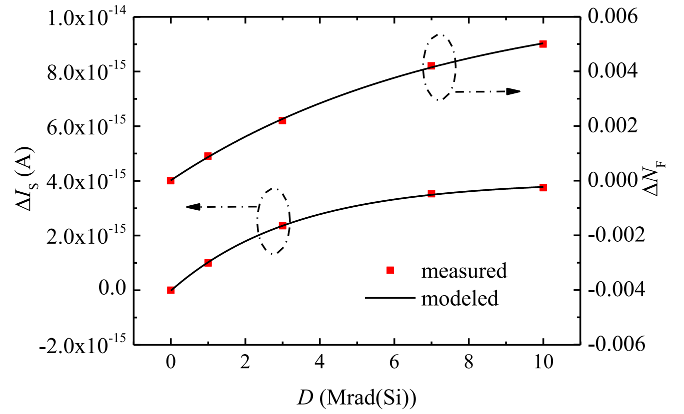

Fig. 4. Measured and modeled results for (a) ΔI_S, (b) ΔN_F.

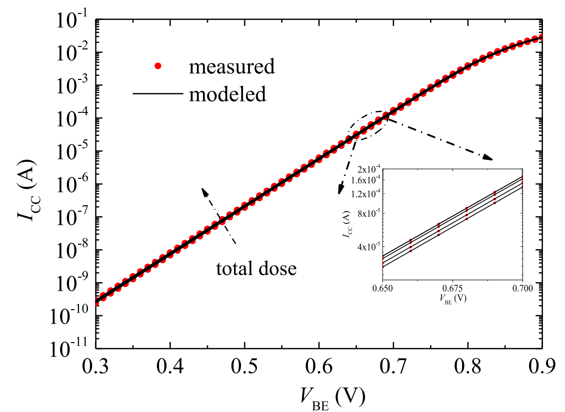

Fig. 5. Measured and modeled results of I_{CC} under different total dose levels.

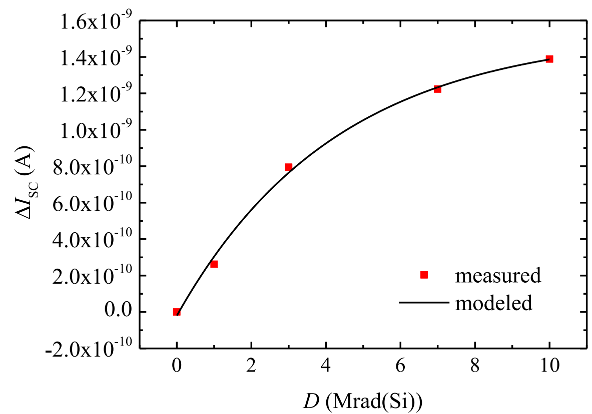

Fig. 6. Measured and modeled results of ΔI_{SC}.

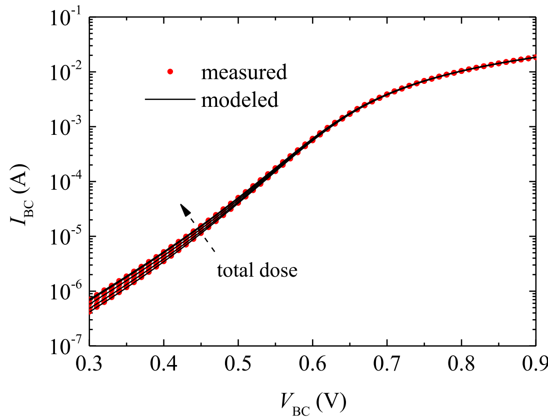

Fig. 7. Measured and modeled results of I_{BC} under different total dose levels.

Compared with I_{BE}-V_{BE} curve, the I_{CC}-V_{BE} curve shows a different behavior as shown in Fig. 5: At all V_{BE} regimes, I_{CC} only shows slight increase.

Gamma-induced excess base current in HBTs is caused by the formation of interface traps. Traps increase carrier recombination in HBTs, primarily within the base region, thereby increasing base current, and the interface traps are created after radiation. Although only the base current at the low V_{BE} regime appear to typical degrade, there are slight degradations in the base current at the high V_{BE} regime and the collector current.

3.2. Inverse Gummel

Model parameters related to the inverse operation follow the same extraction procedure as the forward operation. Table 1 also gives the values of I_{SR}, N_R, I_{SRH}, N_{RH}, I_{SC}, and N_C parameters. It can be observed that only I_{SC} shows slight degradation, and the degradation rate just achieves 81.84% even after 10 Mrad(Si). However, to precisely describe radiation-induced degradation of HBTs, the excess nonideal base-collector saturation current ΔI_{SC} is included in the proposed model, which is not taken account in the model in Ref. [31]. The exponential function expression is also used to describe ΔI_{SC}, as shown in equation (16).

$$\Delta I_{SC} = a_{SC} + b_{SC} \cdot \exp(c_{SC} \cdot D) \tag{16}$$

where a_{SC}, b_{SC}, *and* c_{SC} are fitting parameters.

The measured and modeled curves of ΔI_{SC} versus radiation dose level are shown in Fig. 6. The modeled results agree well with the measured ones, revealing that the adopted expression is effective. The measured and modeled inverse base current I_{BC} versus base-collector bias voltage V_{BC} before and after radiation are presented in Fig. 7. At low biases only the base current I_{BC} increase steadily and slightly with the increase in the radiation dose. Yet, the slope of I_{BC} appears no change for all radiation doses. At high biases the inverse Gummel currents are series-resistance limited and all curves are bunched together, which suggests that no degradation of the series resistances appears. It is believed that gamma-induced excess inverse base current I_{BC} at low biases is caused by radiation-induced defects in the base-collector space charge region and along its periphery [8].

It can be observed that the error between measured and modeled I_{BC} in the all bias range is less than 0.5%. Therefore, we have enough reasons to believe that the proposed improved model for I_{BC} is effective.

3.3. Junction capacitances

The calculation of base-emitter junction capacitance C_{BE} and base-collector junction capacitance C_{BC} are performed using measured so-called "cold-HBT" *S*-parameters. In this case, *S*-parameters are measured at the ground collector and base swept in the range of −2~0 V while emitter is shorted. Next, the *S* parameters are transformed to *Y* parameters. Using the calculated *Y* parameters, C_{BE} and C_{BC} can be obtained by use of equations (17) and (18), respectively.

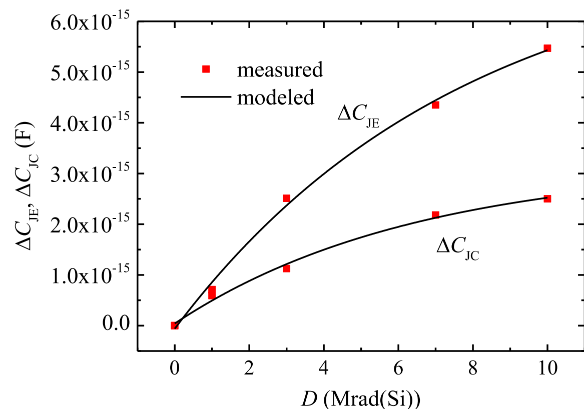

Fig. 8. Measured and modeled results for ΔC_{JE} and ΔC_{JC}.

Table 2
Extracted values of junction-capacitance parameters before and after irradiation.

	Parameters	Pre-radiation	Post-radiation of 1 Mrad (Si)	Post-radiation of 3 Mrad (Si)	Post-radiation of 7 Mrad (Si)	Post-radiation of 10 Mrad (Si)
Base-emitter capacitance	C_{JE} (F)	6.674×10^{-14}	6.745×10^{-14}	6.925×10^{-14}	7.109×10^{-14}	7.221×10^{-14}
	V_{JE} (V)	0.7	0.7	0.7	0.7	0.7
	M_{JE}	0.068	0.068	0.068	0.068	0.068
	C_{Emax} (F)	1.002×10^{-13}	1.002×10^{-13}	1.002×10^{-13}	1.002×10^{-13}	1.002×10^{-13}
	V_{PTE} (V)	3.5	3.5	3.5	3.5	3.5
	M_{JER}	0.05	0.05	0.05	0.05	0.05
Base-collector capacitance	C_{JC} (F)	5.184×10^{-14}	5.243×10^{-14}	5.297×10^{-14}	5.402×10^{-14}	5.434×10^{-14}
	V_{JC} (V)	0.7315	0.7315	0.7315	0.7315	0.7315
	M_{JC}	0.988	0.988	0.988	0.988	0.988
	C_{Cmax} (F)	1.98×10^{-13}	1.98×10^{-13}	1.98×10^{-13}	1.98×10^{-13}	1.98×10^{-13}
	V_{PTC} (V)	1.156	1.156	1.156	1.156	1.156
	M_{JCR}	0.036	0.036	0.036	0.036	0.036

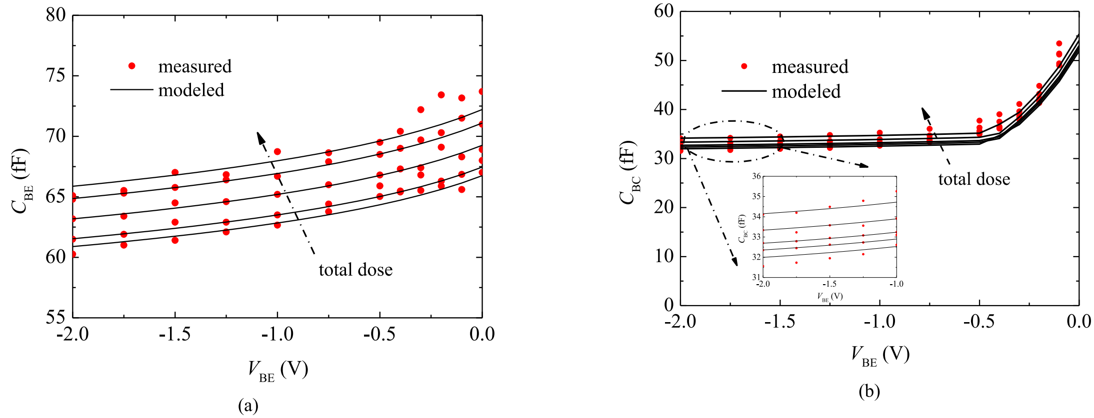

Fig. 9. Measured and modeled results under different total dose levels for (a) C_{BE}, (b) C_{BC}.

Table 3
Extracted values of parameters for transit time before and after irradiation.

Parameters	Pre-radiation	Post-radiation of 1 Mrad (Si)	Post-radiation of 3 Mrad (Si)	Post-radiation of 7 Mrad (Si)	Post-radiation of 10 Mrad (Si)
T_{fb} (S)	5.276×10^{-13}	5.461×10^{-13}	5.638×10^{-13}	5.817×10^{-13}	5.936×10^{-13}
T_{fc0} (S)	3.12×10^{-12}	3.12×10^{-12}	3.12×10^{-12}	3.12×10^{-12}	3.12×10^{-12}
T_{cmin} (S)	2.069×10^{-13}	2.069×10^{-13}	2.069×10^{-13}	2.069×10^{-13}	2.069×10^{-13}
I_{tc} (A)	0.00076	0.00076	0.00076	0.00076	0.00076
I_{tc2} (A)	0.00708	0.00708	0.00708	0.00708	0.00708
V_{tc0Inv} (V)	0.9	0.9	0.9	0.9	0.9
V_{tr0} (V)	3.2	3.2	3.2	3.2	3.2
V_{mx0} (V)	2	2	2	2	2
$V_{tcminInv}$ (V)	0.5	0.5	0.5	0.5	0.5
V_{trmin} (V)	1.2	1.2	1.2	1.2	1.2
V_{mxmin} (V)	1	1	1	1	1
V_{tcInv} (V)	0.4	0.4	0.4	0.4	0.4
V_{tc2Inv} (V)	0.1	0.1	0.1	0.1	0.1
T_{krk} (S)	1.1×10^{-13}	1.1×10^{-13}	1.1×10^{-13}	1.1×10^{-13}	1.1×10^{-13}
I_{krk} (V) (A)	0.0236	0.0236	0.0236	0.0236	0.0236
I_{krktr} (A)	1×10^{-6}	1×10^{-6}	1×10^{-6}	1×10^{-6}	1×10^{-6}
V_{krk} (V)	2.7	2.7	2.7	2.7	2.7
$V_{krk2Inv}$ (V)	0.2	0.2	0.2	0.2	0.2
G_{krk}	4	4	4	4	4
V_{ktr} (V)	0.8	0.8	0.8	0.8	0.8
V_{kmx} (V)	2.4	2.4	2.4	2.4	2.4

$$C_{BE} = \frac{\text{imag}\{Y_{11} + Y_{12}\}}{\omega} \tag{17}$$

$$C_{BC} = \frac{\text{imag}\{-Y_{12}\}}{\omega} \tag{18}$$

Base-emitter and base-collector capacitances calculated from equations (17) and (18) are employed to extract model parameters related with junction capacitances. The C_{JE}, V_{JE}, M_{JE}, C_{Emax}, V_{PTE}, M_{JER}, C_{JC}, V_{JC}, M_{JC}, C_{Cmax}, V_{PTC}, and M_{JCR} parameters of junction capacitances are further estimated by use of optimization method. The extracted junction capacitances parameters for pre-radiation and post-radiation are given in Table 2. Only some slight degradations for C_{JE} and C_{JC} are observed, which validates the correctness of equations (4) and (5) in Section II-C.

In order to describe the increases of C_{JE} and C_{JC}, the following exponential function expressions are adopted to model the excess base-emitter zero-bias capacitance ΔC_{JE} and the excess base-collector zero-bias capacitance ΔC_{JC}:

$$\Delta C_{JE} = a_{JE} + b_{JE} \cdot \exp(c_{JE} \cdot D) \tag{19}$$

$$\Delta C_{JC} = a_{JC} + b_{JC} \cdot \exp(c_{JC} \cdot D) \tag{20}$$

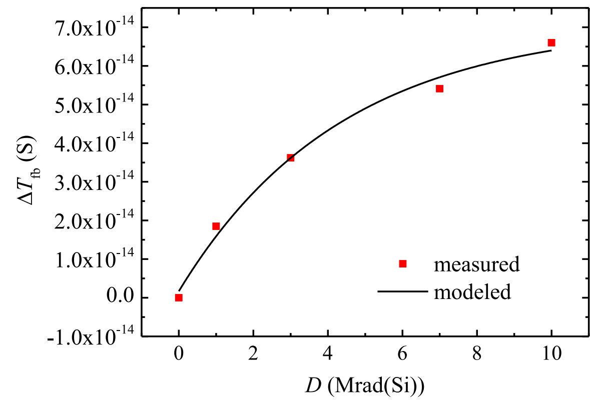

Fig. 10. Measured and modeled results of ΔT_{fb}.

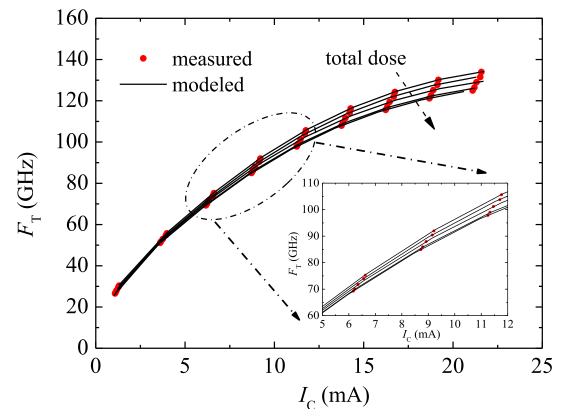

Fig. 11. Measured and modeled results of F_T under different total dose levels.

where a_{JE}, b_{JE}, c_{JE}, a_{JC}, b_{JC}, and c_{JC} are fitting parameters.

The modeled and measured ΔC_{JE} and ΔC_{JC} are illustrated in Fig. 8. It can be observed that the modeled and measured ones fit very well. Fig. 9 shows the success the proposed model when it is used to model experimental results. Slight increases for both C_{BE} and C_{BC} are observed for post-radiation, and they also gradually increase with the increase of radiation dose. Moreover, relatively large degradation occurs in C_{BE}, which suggests that radiation-induced defects in base-emitter junction are more than those in base-collector junction. Since the degradations of C_{BE} and C_{BC} after radiation are very slight, it is feasible that to only improve zero-bias capacitances C_{JE} and C_{JC} to describe the slight degradations, as shown in equations (4) and (5).

3.4. Cutoff frequency

RF performance was obtained by extrapolating −20 dB/decade line from a best-fit average of the current gain (H_{21}), and extraction of H_{21} to 0 dB (unity gain) yield the cutoff-frequency (F_T) of the device. The cutoff frequency F_T for post-radiation of 10 Mrad(Si) represents relatively obvious degradation.

As is discussed in Section III-B, the inverse Gummel currents for high bias ranges almost coincide for pre-radiation and after radiation, suggesting that series resistance have no change even after 10 Mrad(Si) radiation dose. As a couple of factors affecting F_T, slight increases of C_{BE} and C_{BC} are observed in Fig. 9. However, the tiny degradations of junction capacitances are not enough to cause relatively large reduction of F_T. Thus, it is necessary to improve the transit time, which demonstrates the effectiveness of the discussion in Section II-D.

Since we can calculate the transit time from the intercept of $1/(2\pi F_T)$ against the $1/I_C$ curve [31], the cutoff frequency F_T can be used for extracting the transit time related parameters (T_{fb}, T_{fc0}, T_{cmin}, I_{tc}, I_{tc2}, V_{tc0Inv}, V_{tr0}, V_{mx0}, $V_{tcminInv}$, V_{trmin}, V_{mxmin}, V_{tcInv}, V_{tc2Inv}, T_{krk}, I_{krk}, I_{krktr}, V_{krk}, $V_{krk2Inv}$, G_{krk}, V_{ktr}, and V_{kmx}). The optimization fitting method is used to extracted these parameters, whose values are shown in Table III.

From Tables III and it can be easily seen that only T_{fb} appears to slight increase after radiation. The same as the other expressions, ΔT_{fb} can be expressed as equation (21), where a_{fb}, b_{fb}, and c_{fb} are fitting parameters. The measured ΔT_{fb} for all radiation dose levels along with the model curves are presented in Fig. 10, and Fig. 11 shows the measured and modeled F_T for pre-radiation and post-radiation. The good agreement between the measured and modeled F_T with a maximum error less than 0.8% in the all bias regime shows the accuracy of the proposed model.

$$\Delta T_{fb} = a_{fb} + b_{fb} \cdot \exp(c_{fb} \cdot D) \tag{21}$$

4. Conclusion

A novel radiation-dependence model of InP HBTs including gamma radiation effects has been proposed in this paper. To predict characteristics of devices/circuits in the space radiation environment, some empirical expressions incorporated into the novel model have been proposed. To validate the effective of the proposed model, a series of radiation experiment has been performed. The experimental and simulated results show that the model can precisely model the radiation-induced degradations in forward Gummel currents, inverse Gummel currents, junction capacitances and cutoff frequency.

Declaration of competing interest

We declare that we have no financial and personal relationships with other people or organizations that can inappropriately influence our work, there is no professional or other personal interest of any nature or kind in any product, service and/or company that could be construed as influencing the position presented in, or the review of, the manuscript entitled: "A novel radiation-dependence model of InP HBTs including gamma radiation effects"

References

[1] A. Zhang, J. Gao, An improved nonlinear model for millimeter-wave InP HBT including DC/AC dispersion effects, IEEE Microw. Wireless Compon. Lett. 31 (5) (May 2021) 465–468, https://doi.org/10.1109/LMWC.2021.3068145.

[2] Z. Liu, T. Sharma, K. Sengupta, 80–110-GHz broadband linear PA with 33% peak PAE and comparison of stacked common base and common emitter PA in InP, IEEE Microw. Wireless Compon. Lett. 31 (6) (June 2021) 756–759, https://doi.org/10.1109/LMWC.2021.3067233.

[3] J. Kim, et al., Terahertz signal source and receiver operating near 600 GHz and their 3-D imaging application, IEEE Trans. Microw. Theor. Tech. 69 (5) (May 2021) 2762–2775, https://doi.org/10.1109/TMTT.2021.3061596.

[4] Z. Liu, T. Sharma, C.R. Chappidi, S. Venkatesh, Y. Yu, K. Sengupta, A 42–62 GHz transformer-based broadband mm-wave InP PA with second-harmonic waveform engineering and enhanced linearity, IEEE Trans. Microw. Theor. Tech. 69 (1) (Jan. 2021) 756–773, https://doi.org/10.1109/TMTT.2020.3037092.

[5] X.H. Zhao, H.L. Lu, Y.M. Zhang, et al., The impact of laser energy, bias and irradiation positions on single event transients of InP HBT, J. Phys. D Appl. Phys. 53 (14) (Apr. 2020), 145104, https://doi.org/10.1088/1361-6463/ab6622.

[6] M. Liu, Y.M. Zhang, H.L. Lu, et al., Investigation of proton irradiation effects on InP/InGaAs double heterojunction bipolar transistors, Solid State Electron. 109 (July 2015) 52–57, https://doi.org/10.1016/j.sse.2015.03.008.

[7] F.S. Minko, T. Stander, Effect of TID electronradiation on SiGe BiCMOS LNAs at V-band, Microelectron. Reliab. 112 (Sep. 2020), 113750, https://doi.org/10.1016/j.microrel.2020.113750.

[8] J.C. Zhang, K. Xu, J.C. Wang, et al., Modeling and analysis for the effects of gamma irradiation on the DC and AC performance in InGaP/GaAs SHBTs, Radiat. Eff. Defect Solid 175 (5–6) (May 2020) 492–503, https://doi.org/10.1080/10420150.2019.1684916.

[9] J.X. Zhang, Q. Guo, H.X. Guo, et al., Investigation of enhanced low dose rate sensitivity in SiGe HBTs by Co-60 gamma irradiation under different biases, Microelectron. Reliab. 84 (May 2018) 105–111, https://doi.org/10.1016/j.microrel.2018.03.007.

[10] S.H. Liu, A. Hussain, D. Li, et al., Total ionizing dose effects of SiGe HBTs induced by Co-60 Gamma-ray irradiation, Nucl. Sci. Eng. 191 (1) (98–103 (2018, https://doi.org/10.1080/00295639.2018.1450004.

[11] J. Schmidt, J. Korn, G.G. Fischer, et al., Impact of breakdown voltage on gamma irradiation effects in 0.13-μm and 0.25-μm SiGe HBTs, IEEE Trans. Nucl. Sci. 64 (4) (Apr. 2017) 1037–1041, https://doi.org/10.1109/tns.2017.2682927.

[12] J.N. Wei, C.H. He, P. Li, et al., Impact of displacement damage on single event transient charge collection in SiGe HBTs, Nucl. Instrum. Methods Phys. Res. Sect. A Accel. Spectrom. Detect. Assoc. Equip. 938 (Sep. 2019) 29–35, https://doi.org/10.1016/j.nima.2019.05.098.

[13] O.M. Lawal, Z. Li, S. Liu, et al., Experimental study of pulse neutron irradiation damage in SiGe HBT, J. Nucl. Sci. Technol. 55 (12) (Dec. 2018) 1425–1433, https://doi.org/10.1080/00223131.2018.1512427.

[14] Y.B. Sun, Z.Y. Liu, J. Fu, et al., Degradation and annealing characteristics of NPN SiGe HBT exposed to heavy ions irradiation, Radiat. Phys. Chem. 165 (Dec. 2019), 108433, https://doi.org/10.1016/j.radphyschem.2019.108433.

[15] V.N. Hegde, K.C. Praveen, T.M. Pradeep, et al., High energy swift heavy ion irradiation and annealing effects on DC electrical characteristics of 200 GHz SiGe HBTs, Nucl. Eng. Technol. 51 (5) (Aug. 2019) 1428–1435, https://doi.org/10.1016/j.net.2019.03.016.

[16] J.X. Zhang, H.X. Guo, F.Q. Zhang, et al., Heavy ion micro-beam study of single-event transient (SET) in SiGe heterjunction bipolar transistor, Sci. China Inf. Sci. 60 (12) (Dec. 2017), 120404, https://doi.org/10.1007/s11432-017-9249-6.

[17] Y.B. Sun, J. Fu, J. Xu, et al., Comparison of total dose effects on SiGe heterojunction bipolar transistors induced by different swift heavy ion irradiation, Chin. Phys. B 23 (11) (Nov. 2014), 116104, https://doi.org/10.1088/1674-1056/23/11/116104.

[18] J.N. Wei, C.H. He, P. Li, et al., Impact of layout and profile optimization for inverse-mode SiGe HBT on SET and TID responses, Microelectron. Reliab. 105 (Feb. 2020), 113561, https://doi.org/10.1016/j.microrel.2019.113561.

[19] Z. Zhao, N.Y. Jiang, Z.Q. Ma, et al., Impact of finger numbers on the performance of proton-radiated SiGe power HBTs at room and cryogenic temperatures, Microelectron. Reliab. 91 (Dec. 2018) 194–200, https://doi.org/10.1016/j.microrel.2018.10.006.

[20] K.O. Petrosyants, M.V. Kozhukhov, Physical TCAD model for proton radiation effects in SiGe HBTs, IEEE Trans. Nucl. Sci. 63 (4) (Aug. 2016) 2016–2021, https://doi.org/10.1109/tns.2016.2572658.

[21] C.H. Li, H.L. Lu, Y.M. Zhang, et al., Proton-induced degradation of InP/InGaAs HBTs predicted by nonionizing energy loss model, IEEE Trans. Nucl. Sci. 62 (3) (Jun. 2015) 1336–1340, https://doi.org/10.1109/tns.2015.2416729.

[22] M. Liu, Y.M. Zhang, H.L. Lu, et al., Proton irradiation effects on InGaP/GaAs single heterojunction bipolar transistors, Solid State Electron. 96 (Jun. 2014) 9–13, https://doi.org/10.1016/j.sse.2014.03.010.

[23] Z.E. Fleetwood, A. Ildefonso, G.N. Tzintzarov, et al., SiGe HBT profiles with enhanced inverse-mode operation and their impact on single-event transients, IEEE Trans. Nucl. Sci. 65 (1) (Jan. 2018) 399–406, https://doi.org/10.1109/TNS.2017.2782183.

[24] N.E. Lourenco, Z.E. Fleetwood, A. Ildefonso, et al., The impact of technology scaling on the single-event transient response of SiGe HBTs, IEEE Trans. Nucl. Sci. 64 (1) (Jan. 2017) 406–414, https://doi.org/10.1109/TNS.2016.2633997.

[25] N.E. Lourenco, A. Ildefonso, G.N. Tzintzarov, et al., Single-event upset mitigation in a complementary SiGe HBT BiCMOS technology, IEEE Trans. Nucl. Sci. 65 (1) (Jan. 2018) 231–238, https://doi.org/10.1109/TNS.2017.2778803.

[26] P. Li, M.H. Liu, C.H. He, et al., An investigation of ionizing radiation damage in different SiGe processes, Chin. Phys. B 26 (8) (Aug. 2017), 088503, https://doi.org/10.1088/1674-1056/26/8/088503.
[27] J.X. Zhang, Q. Guo, H.X. Guo, et al., Impact of bias conditions on total ionizing dose effects of 60Coγ in SiGe HBT, IEEE Trans. Nucl. Sci. 63 (2) (April 2016) 1251–1258, https://doi.org/10.1109/TNS.2016.2522158.
[28] A. Bandyopadhyay, S. Subramanian, S. Chandrasekhar, et al., Degradation of DC characteristics of InGaAs/InP single heterojunction bipolar transistors under electron irradiation, IEEE Trans. Electron. Dev. 46 (5) (May 1999) 840–849, https://doi.org/10.1109/16.760388.
[29] A. Bandyopadhyay, S. Subramanian, S. Chandrasekhar, et al., Degradation of InGaAs/InP double heterojunction bipolar transistors under electron irradiation, IEEE Trans. Electron. Dev. 46 (5) (May 1999) 850–858, https://doi.org/10.1109/16.760389.
[30] J.C. Zhang, Y.M. Zhang, H.L. Lu, et al., The model parameter extraction and simulation for the effects of gamma irradiation on the DC characteristics of InGaP/GaAs single heterojunction bipolar transistors, Microelectron. Reliab. 52 (Dec. 2012) 2941–2947, https://doi.org/10.1016/j.microrel.2012.07.020.
[31] J.C. Zhang, Y.M. Zhang, H.L. Lu, et al., A novel model for implementation of gamma radiation effects in GaAs HBTs, IEEE Trans. Microw. Theor. Tech. 60 (12) (Dec. 2012) 3693–3698, https://doi.org/10.1109/TMTT.2012.2221137.
[32] J.C. Zhang, M. Liu, J.C. Wang, et al., Modeling of InP HBTs with an improved Keysight HBT model, Microw. J. 62 (7) (Jul. 2019) 56–62.
[33] J.C. Zhang, L. Cao, M. Liu, et al., Gamma-induced degradation effect of InP HBTs studied by Keysight model, Nucl. Sci. Eng. 195 (2) (Feb. 2021) 173–184, https://doi.org/10.1080/00295639.2020.1798679.
[34] J.C. Zhang, B. Liu, L.W. Zhang, et al., A rigorous peeling algorithm for direct parameter extraction procedure of HBT small-signal equivalent circuit, Analog Integr. Circuits Signal Process. 85 (3) (Dec. 2015) 405–411, https://doi.org/10.1007/s10470-015-0586-z.